Journal of Power Sources 293 (2015) 649–656

Contents lists available at ScienceDirect

Journal of Power Sources

journal homepage: www.elsevier.com/locate/jpowsour

Selective deposition of nanostructured ruthenium oxide using Tobacco mosaic virus for micro-supercapacitors in solid Nafion electrolyte

Markus Gnerlich [a, *], Hadar Ben-Yoav [a, b], James N. Culver [c, d], Douglas R. Ketchum [e], Reza Ghodssi [a, b]

[a] Dept. of Electrical and Computer Engineering, 2410 A.V. Williams Building, University of Maryland, College Park, MD 20742, United States
[b] Institute for Systems Research, 2173 A.V. Williams Building, University of Maryland, College Park, MD 20742, United States
[c] Institute for Bioscience and Biotechnology Research, Plant Sciences Building, University of Maryland, College Park, MD 20742, United States
[d] Dept. of Plant Science and Landscape Architecture, 2102 Plant Sciences Building, University of Maryland, College Park, MD 20742, United States
[e] Laboratory for Physical Sciences, 8050 Greenmead Drive, College Park, MD 20742, United States

HIGHLIGHTS

- A method of selective patterning of RuO_2 on microelectrodes is described.
- The microelectrodes consist of titanium nitride with Au and Ni functional areas.
- Micro-supercapacitors in solid Nafion electrolyte are tested.
- Electrode capacitance has been measured as high as 203 mF cm^{-2}.
- The presence of Tobacco mosaic virus nanotemplate improves rate capability.

ARTICLE INFO

Article history:
Received 10 March 2015
Received in revised form
3 May 2015
Accepted 15 May 2015
Available online 6 June 2015

Keywords:
Supercapacitor
Ruthenium oxide
Tobacco mosaic virus
Electroless deposition
Self-assembly
Nafion

ABSTRACT

A three-dimensional micro-supercapacitor has been developed using a novel bottom-up assembly method combining genetically modified *Tobacco mosaic* virus (TMV-1Cys), photolithographically defined micropillars and selective deposition of ruthenium oxide on multi-metallic microelectrodes. The three-dimensional microelectrodes consist of a titanium nitride current collector with two functionalized areas: (1) gold coating on the active electrode area promotes TMV-1Cys adhesion, and (2) sacrificial nickel pads dissolve in ruthenium tetroxide plating solution to produce ruthenium oxide on all electrically connected areas. The microfabricated electrodes are arranged in an interdigitated pattern, and the capacitance per electrode has been measured as high as 203 mF cm^{-2} with solid Nafion electrolyte. The process integration of bio-templated ruthenium oxide with microfabricated electrodes and solid electrolyte is an important advance towards the energy storage needs of mass produced self-sufficient micro-devices.

1. Introduction

Integration of capacitors, inductors and resistors with micro-electronics is attractive due to the decreased overall size, reduced packaging compared to discrete devices, and increased reliability due to fewer chip-to-chip and chip-to-board connections. The addition of integrated energy-storage elements would further decrease size and lead to an anticipated revolution of micro-sized self-sufficient devices. The use of solid electrolyte allows this miniaturization to proceed without complex packaging steps needed for application and sealing of liquid electrolyte. All-solid micro-supercapacitors have the potential to fill the energy-storage need due to their high power density, low maintenance and long cycle-lifetimes.

The characteristic features of micro-supercapacitors are defined by the microfabrication methods used to produce them. Traditional

* Corresponding author. 8050 Greenmead Drive, College Park, MD 20742, United States.
E-mail address: gnerlich@lps.umd.edu (M. Gnerlich).

http://dx.doi.org/10.1016/j.jpowsour.2015.05.053
0378-7753/

energy storage devices are constructed with facing electrode plates and an electrolyte sandwiched between them, but this is a highly challenging geometry when using photolithographically defined layers. Instead, electrode plates are arranged in the same plane and defined with an interdigitated geometry to reduce diffusion lengths through the electrolyte. It is desirable to increase surface area for two reasons. First, the effective capacity of redox materials is closely related to the penetration depth of the electrolyte ions. Second, the overall mass loading is increased for surface deposition methods such as electroless plating. The combination of high surface area and thin materials leads to both higher energy and power densities.

Ruthenium oxide (RuO_2) has been intensely studied as a redox material for electrochemical supercapacitors due to its high gravimetric capacity. Anhydrous RuO_2 is an electronic conductor with high stability and chemical resistance, but it conducts H^+ ions when prepared as $RuO_2 \cdot xH_2O$. The H^+ conduction allows a reduction–oxidation reaction to occur within the bulk of the material, not just on the surface, resulting in high gravimetric capacitance. The methods of preparation, chemical and physical structure of $RuO_2 \cdot xH_2O$ have been extensively researched [1–5]. Interestingly, RuO_4 is used as an electron microscopy stain due to the deposition of conductive RuO_2 nanoscrystals in biological tissues and plastics. RuO_2 films can be deposited on surfaces by vapor phase RuO_4 [6], and methods for selective deposition of $RuO_2 \cdot xH_2O$ from vapor phase RuO_4 have been developed [7]. When $RuO_2 \cdot xH_2O$ possesses nanoscale dimensions and is in contact with a good current collector, gravimetric capacitances over 1000 F g-1 have been reported. For instance, ruthenium oxide powder mixed with activated carbon black [8], colloidal ruthenium oxide loaded on carbon powder [9], sol-gel-derived ruthenium oxide nanoparticles on carbon powder [10], ruthenium oxide nanotubes [11], and facile ruthenium oxide nanoparticles on carbon powder [12] have all been found to display such gravimetric capacitances. In addition, the role of mesoporous structure in anhydrous RuO_2 capacitance has been investigated [13], and RuO_2 and $RuO_2 \cdot xH_2O$ powders with nanoscale dimensions have also been similarly studied [14]. The authors direct the reader to a review [15] of nanostructured materials in electrochemical supercapacitors for more information about this field.

A well-known disadvantage of RuO_2 is the cost, but material expense is often secondary to performance when considered in terms of the overall microfabrication expense. Due to the inherent challenges of microfabrication process integration, there are far fewer reported breakthroughs with RuO_2 micro-supercapacitors than with RuO_2 electrodes prepared by bulk synthesis methods. A mix of RuO_2 nanorods and $RuO_2 \cdot xH_2O$ on interdigitated electrodes produced supercapacitors with 12–41 mF cm^{-1} in aqueous 0.5M H_2SO_4 electrolyte [16], and electrodeposition of hydrous RuO_2 onto gold microelectrodes was reported at 0.2 mF cm^{-1} in aqueous 0.5M H_2SO_4 electrolyte [17]. Recently, electrodeposition of hydrous RuO_2 on a high-aspect-ratio silicon microtemplate produced electrodes with 92 mF cm^{-2} (or 23 mF cm^{-2} based on device footprint) in neutral aqueous 0.1M Na_2SO_4 electrolyte [18], and this value was increased to 148 mF cm^{-2} (or 37 mF cm^{-2} based on device footprint) by introducing CNT into the deposition process [19]. Few reports exist on the full integration of micro-electrodes with a solid electrolyte, which is desirable to avoid the complex packaging methods for a liquid electrolyte. This is surprising despite work on RuO_2 with Nafion solid electrolyte in traditional sandwich structures [20], [21]. One such rare device in solid electrolyte is based on polypyrrole micro-electrodes which were reported at 29–60 mF cm^{-2} in hydrated PVA gel with $LiClO_4$ [22]. A related technology is carbon-based EDL capacitors (without redox material) using organic electrolytes. Silicon microwells have been used as a template for activated carbon with resulting capacitance of 91 mF cm^{-2} [23]. A useful summary of micro-supercapacitor values is found in Table 2 [23]. Notably, the challenging aspect of encapsulating activated carbon micro-electrodes with liquid organic electrolyte (1M Et_4NBF_4 into propylene carbonate) has been described with capacitance of 81 mF cm^{-2} [24].

The micro-supercapacitor described here uses a novel bottom-up assembly method combining genetically modified *Tobacco mosaic* virus (TMV-1Cys), photolithographically defined micropillars and selective deposition of RuO_2 on multi-metallic microelectrodes. The 3D microelectrodes consist of a titanium nitride current collector with two functionalized areas: (1) gold coating on the active electrode area promotes TMV-1Cys adhesion, and (2) sacrificial nickel pads dissolve in RuO_4 plating solution to selectively deposit RuO_2 on all electrically connected areas. The *T. mosaic* virus has a cylindrical structure (300 nm by 18 nm) and functions as a nanotemplate for the RuO_2 coating. The genetically modified TMV variant (TMV-1Cys) contains an additional cysteine amino acid in the coat protein, which improves electrolessly deposited metallic coatings through the presence of the thiol side chain present on each of the more than 2100 coat proteins that comprise one virus particle [25]. The resulting micro-supercapacitor is tested with solid Nafion perfluorosulfonate ionomer. Incorporation of solid electrolyte is an important aspect of the process integration since it significantly reduces packaging complexity and improves device stability. Related work with TMV-1Cys has used TMV-1Cys/Ni as a template for battery electrodes [26], and RuO_2 deposited by ALD has been tested on a TMV-1Cys/Ni/TiN template [27]. The engineering applications of TMV have been extensively reviewed [28] as well as the biological approaches using self-assembly for producing nanomaterials [29].

2. Materials and methods

2.1. Fabrication

The fabrication process for the micro-supercapacitors is based on metal electrodes on a polyimide insulating substrate which are photolithographically defined on 3-inch silicon wafers. The layout of a typical device is shown in Fig. 1 (a). The result of the TMV-1Cys/RuO_2 coating method (see in Fig. 1 (b,c)) is a forest-like surface of hydrated $RuO_2 \cdot xH_2O$ covering the micropillars and TMV-1Cys biotemplate (see Fig. 2). For simplicity, micropillars are not shown in the cross-section diagrams.

Fabrication started with a 5 μm spin-coated film of HD-4100 polyimide precursor (HD Microsystems) that was flood exposed, followed by a 5 μm coat exposed with a mask to define 4 μm diameter micropillars. The HD-4100 polyimide precursor was baked in a vacuum oven at 200 °C for 1 h followed by 375 °C for 90 min. Next, Ti/Au (500 Å/2000 Å) was deposited in an e-beam evaporator (CH Industries Mark-40). A Ti/TiN (1000 Å/1000 Å) layer was deposited by RF sputtering in an Ar/N_2 gas mixture (Trikon Sigma 200). A final Ti/Au (50 Å/750 Å) layer was deposited in an e-beam evaporator. The titanium nitride acts as a chemically resistant coating, and the top gold provides good adhesion for the TMV-1Cys biotemplate.

Nickel (5000 Å) deposited in an e-beam evaporator was used as a hard mask, and the layer was defined with AZ nLOF 2035 lift-off photoresist. The electrodes were etched in a PlasmaTherm 790 series reactive ion etcher using four steps. First, the top gold layer was sputter etched in Ar plasma. Second, the Ti/TiN/Ti layers were etched in SF_6 plasma, and a hydrogen plasma etch was used to remove fluorine-containing residue. Third, the bottom Au layer was removed in another Ar plasma sputter etch. Finally, the thin Ti adhesion layer was removed in a short CHF_3 plasma etch.

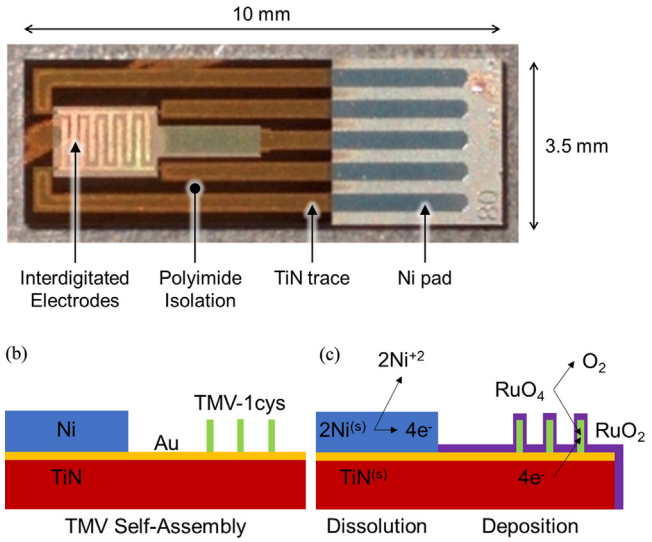

Fig. 1. (a) Photograph of a single chip with interdigitated micro-electrodes and electrode area of 2.00 mm by 1.25 mm, or the same size as a 0805 surface-mount component. (b) The TMV-1Cys/RuO_2 coating process on TiN/Ni electrodes starts with TMV-1cys assembly on the Au coated TiN electrodes and adheres by thiol bond to cysteine in the coat protein. (c) Next, nickel is used as a sacrificial metal during the reduction of RuO_4 to RuO_2 on the surface of the electrode in the presence of TMV-1cys. Both nickel and gold can be dissolved in the RuO_4 solution, but titanium nitride is chemically stable and adheres well to RuO_2.

Afterwards, Transene Nickel Etchant TFG at 40 °C was used to selectively removed Ni from the electrode area after a photoresist pattern (AZ 9260) was defined. A final cleanup was performed with photoresist stripper and an oxygen plasma descum.

After wafer dicing, the 3.5 mm by 10 mm chips were submerged in a suspension of TMV-1Cys (0.2 mg ml^{-1}) in 1.0M phosphate buffer, and a few seconds of sonication was used to remove any surface bubbles. The TMV-1Cys coating method is based on the work of Gerasopoulos et al. [26]. During the 16 h coating process, the chips were refrigerated at 4 °C and the TMV-1Cys self-assembled on Au-coated TiN electrodes. A thiol bond occurs between the cysteine amino acid in the virus coat protein and the gold surface, immobilizing the virus particles. Next, the chips were dip-rinsed in DI water to remove excess material and submerged in fresh 0.5% RuO_4 solution (Polysciences) that was brought to room temperature. Note that RuO_4 is volatile and a strong oxidizer that must be handled with care. RuO_4 produces hazardous vapor at room temperature and must be used in a fume hood with appropriate PPE. A visible coating of RuO_2 formed on the electrodes due to two simultaneous reactions. As shown in the schematic diagram in Fig. 1 (b,c), nickel dissolves on the pad region of the electrically connected electrode by $2Ni^{(s)} \rightarrow 2Ni^{+2} + 4e^-$, and ruthenium tetroxide is reduced on the electrode region by $RuO_4 + 4e^- \rightarrow RuO_2^{(s)} + O_2$. The TiN acts as a chemically stable support during the coating process since even gold can be removed in the strongly oxidizing RuO_4 solution. However, it was found that without a gold surface layer, the TMV-1Cys does not produce a dense coating and without TiN, the RuO_2 film adheres poorly and delaminates during the subsequent drying step. Furthermore, the presence of micropillars mechanically secures the film, significantly reducing large cracks and preventing delamination during the drying and annealing steps. After 5–20 min the chips were rinsed in DI water and dried under nitrogen.

A gap of 96 μm exists between pairs of interdigitated electrodes with a "finger" dimension of 96 × 992 μm. The gap was partially filled by lateral growth adjacent to the electrodes and estimated to be approximately 10 μm based on SEM observation and EDX line-scan, leading to a fill factor of 60% based on electrode geometry. The overall device footprint is 0.025 cm^2 with each electrode occupying 0.00754 cm^2. These values were used for the calculation of current

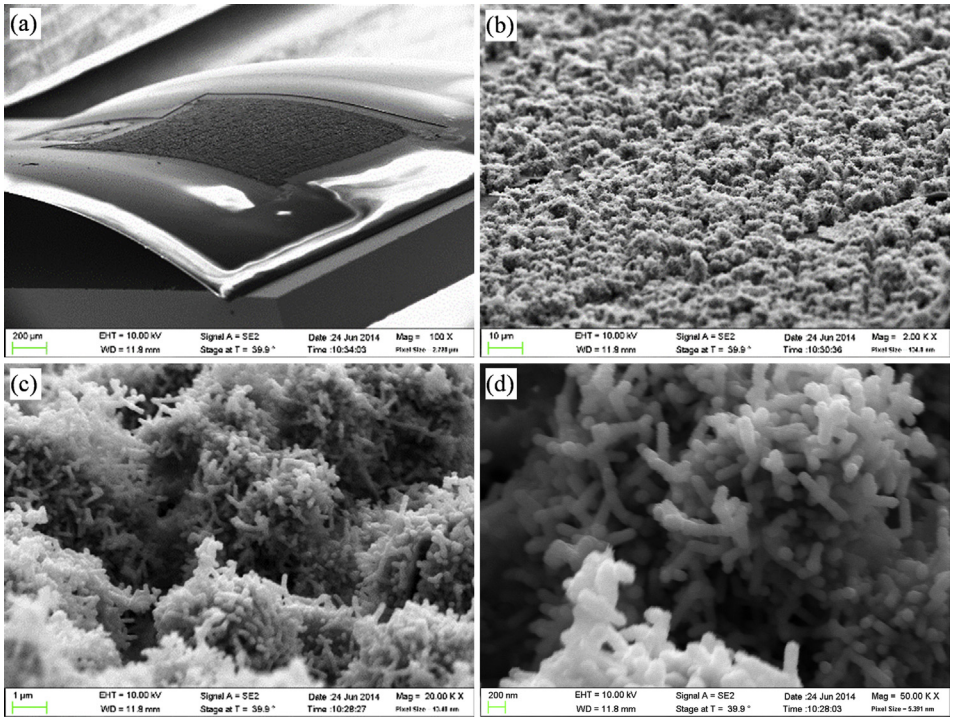

Fig. 2. SEM image of a flexible polyimide substrate with TMV-1Cys/RuO_2 coated titanium nitride microelectrodes. The array of 5 μm tall micropillars are obscured by the thick TMV-1Cys/RuO_2 coating, but impart a periodic appearance to the surface. The diameter of the nanorods attached to the 3D electrode surface is approximately 150 nm.

density and areal capacity. The mass of RuO_2 could not be determined since RuO_2 deposition occurs simultaneously with erosion of the sacrificial Ni, therefore gravimetric values of RuO_2 are not reported.

The devices were baked in a clean-room oven at 150 °C for 12 h in order to optimize the water content in the $RuO_2 \cdot xH_2O$ coating. Devices tested in solid electrolyte were coated with Nafion dispersion (Ion Power D2021) by drop casting on the electrode area. The dispersion was allowed to dry at ambient conditions for approximately 30 min. The devices were then annealed again in a nitrogen purged ramping oven at 70 °C for 2 h and 150 °C for 4 h.

2.2. Electrochemical test

The finished chips were designed to fit in the slot of a standard micro-USB plug to facilitate rapid testing of the micro-supercapacitors. Electrochemical tests in aqueous 1.0M H_2SO_4 electrolyte were completed with a Ag/AgCl reference electrode and Pt foil counter electrode. A BioLogic VSP potentiostat was used for cyclic voltammetry and chronopotentiometry; the results were analyzed in BioLogic EC-Lab v10.37 software. For testing in solid Nafion electrolyte, the micro-supercapacitors were mounted in sockets connected to a PCB that was in turn connected to the BioLogic VSP potentiostat. The PCB was housed in a controlled temperature and humidity chamber (Espec SH-241) set at 25 °C and 80% relative humidity. Nafion electrolyte requires a level of hydration in order to perform well, and 80% was chosen based on reported values of ionic conductivity as a function of relative humidity and water uptake [30]. Since the interdigitated electrodes are coated with a film of solid electrolyte, there is no room for an external reference electrode. The micro-supercapacitors are tested in symmetric 2-electrode configuration; this is standard practice for supercapacitor testing. Energy storage capacity was calculated in EC-Lab by using a feature to automatically compute the total discharge (Q) per cycle. Capacitance was measured as Q divided by the maximum test voltage of 800 mV. Since each electrode is in series in the 2-electrode configuration, the capacitance of the tested device is one-half that of the individual electrodes. Unless stated otherwise, the reported areal capacitance values represent the value for each individual electrode.

3. Results and discussion

The combination of micro-pillars, nanoscale TMV-1Cys and selective coating of RuO_2 on electrode areas has produced a microfabrication method with a number of benefits. The coatings are specific to the micro-electrode areas without the need for physical templating or etch-back steps. The substrate does not require a seed layer or any external electrical current source during the deposition process as is typical with electroplating. The plating reaction stops when the sacrificial nickel is exhausted providing a straightforward means of controlling thickness. Finally, the combination of selective coating and integration with a solid electrolyte is highly advantageous for microelectronics applications. This system produced a capacitance measurement of 203 mF cm^{-2} with a solid Nafion electrolyte, demonstrating excellent energy storage capacity for a thin solid micro-supercapacitor.

The selective coating of RuO_2 on the microelectrodes was verified by SEM and EDX spectral imaging (see Fig. 3), and the RuO_2 coating is specific to the electrode area. The titanium nitride electrodes are covered with ruthenium, while the carbon-containing polyimide is still visible between the interdigitated electrodes. The ability to selectively coat electrodes is the critical feature of this process since it allows process integration without the need for an electroplating seed layer, and without the material waste of etching RuO_2. The electrical separation of the interdigitated electrodes is confirmed by the low leakage current value reported below.

The rate capability of the solid micro-supercapacitors was measured by cyclic voltammetry with scan rates between 0.5 and 250 mV sec^{-1}. A comparison between solid Nafion electrolyte and aqueous 1.0M H_2SO_4 electrolyte is shown in Fig. 4 (a). The electrodes in 1.0M H_2SO_4 were tested against a Ag/AgCl reference, and

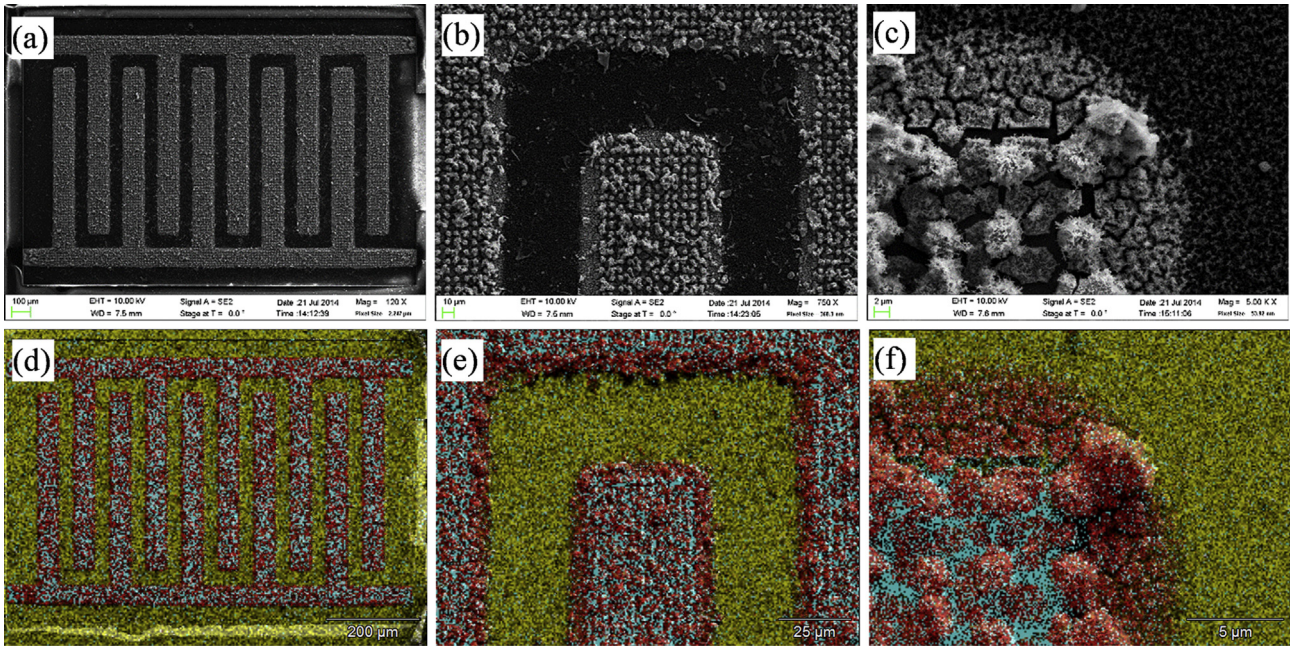

Fig. 3. SEM and EDX spectral map at (a,d) 120X, (b,e) 750X and (c,f) 5000X where red = ruthenium, yellow = carbon, and cyan = titanium. The selective deposition of TMV-1Cys/RuO_2 can be seen on the microelectrodes while the polyimide area is uncoated (For interpretation of the references to color in this figure legend, the reader is referred to the web version of this article.).

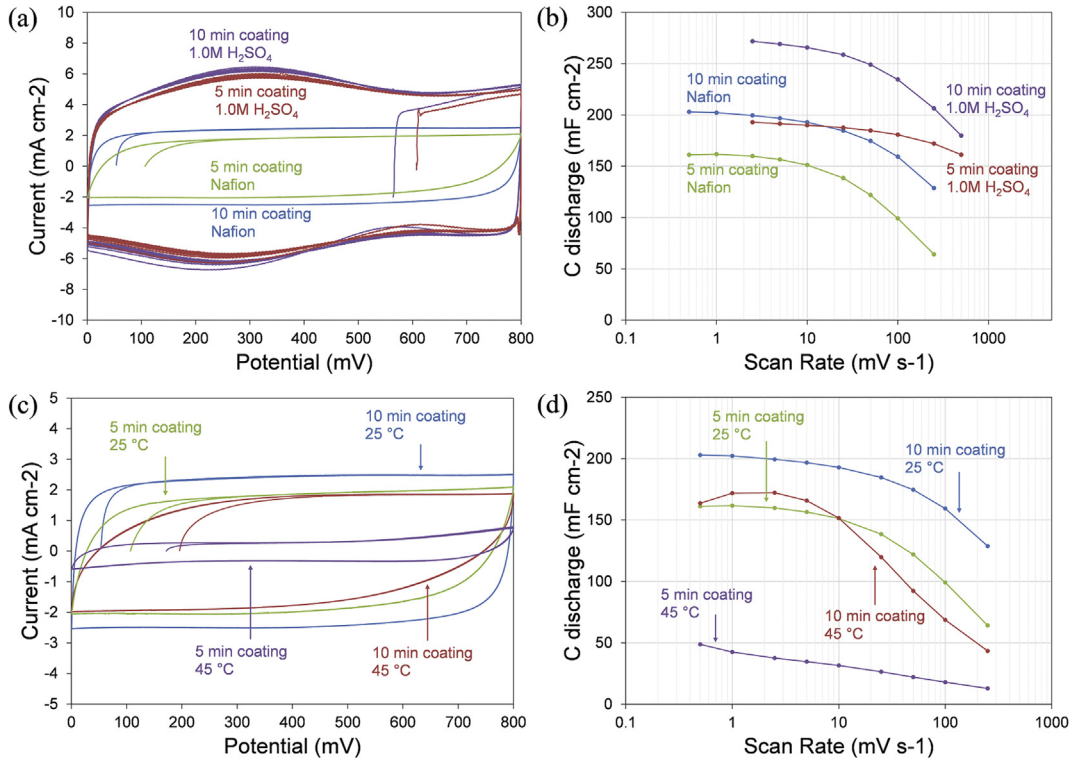

Fig. 4. (a) Cyclic voltammetry at 25 mV s^{-1} and (b) rate dependence results for samples tested in Nafion electrolyte at 25 °C and 80% RH with comparison to 1.0M H_2SO_4 electrolyte. The electrodes in 1.0M H_2SO_4 were tested against a Ag/AgCl reference, and the electrodes in Nafion were tested in a 2-electrode configuration without a reference. (c) Cyclic voltammetry at 25 mV s^{-1} and (d) rate dependence results for samples tested in Nafion electrolyte after the temperature was increased to 45 °C at 80% RH.

the electrodes in Nafion were tested in a 2-electrode configuration without a reference. The absence of redox peaks is typical when measured in a 2-electrode configuration [31]. The corresponding comparison of discharge capacitance as a function of scan rate is shown in Fig. 4 (b). A value of 199 mF cm^{-2} was measured at 2.5 mV s^{-1} with solid Nafion electrolyte, which compares very favorably to 272 mF cm^{-2} at 2.5 mV s^{-1} in aqueous 1.0M H_2SO_4 electrolyte at 2.5 mV s^{-1}. Despite moving to a solid electrolyte, devices in Nafion retained 73% of the areal capacitance when compared to aqueous electrolyte. The maximum recorded areal capacitance of the micro-supercapacitor electrode was 203 mF cm^{-2} at 0.5 mV s^{-1}, which is an excellent value for interdigitated micro-electrodes in a solid electrolyte. The corresponding capacitance of a full device which occupies the 0.025 cm^2 footprint of a standard 0805 SMD was 765 μF. In order to explore the effect of increased temperature on the micro-supercapacitors, the cyclic-voltammetry tests of electrodes in Nafion were repeated at 45 °C and 80% RH. The shape of the curves in Fig. 4 (c) did not change significantly although redox peaks would be difficult to discern in a 2-electrode configuration. A comparison of discharge capacitance as a function of scan rate is shown in Fig. 4 (d), and the increase in temperature caused a significant loss of capacity in Nafion electrolyte. The effects of temperature are discussed further below with regard to EIS measurements.

The supercapacitors were also tested by chronopotentiometry with current density between 3.3 μA cm^{-2} and 33 mA cm^{-2} (Fig. 5 (a)), which corresponds to a C-rate up to approximately 1000 (Fig. 5 (b)). At the highest current densities, the limiting factor is believed to be the conduction of the current collector because at 33 mA cm^{-2} the capacity retention of electrodes coated for 5 min was 1% while

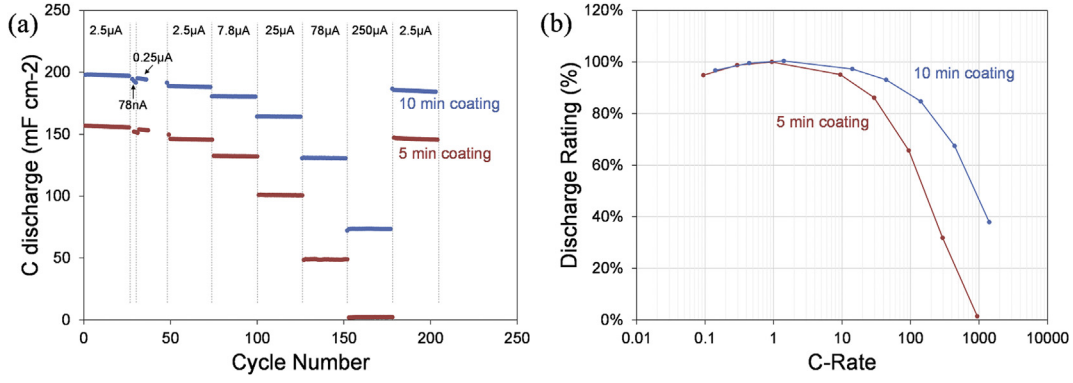

Fig. 5. Rate capability shown as (a) discharge capacity versus cycle number and (b) percentage of 1 C value versus C-rate for devices tested in Nafion electrolyte (25 °C and 80% RH).

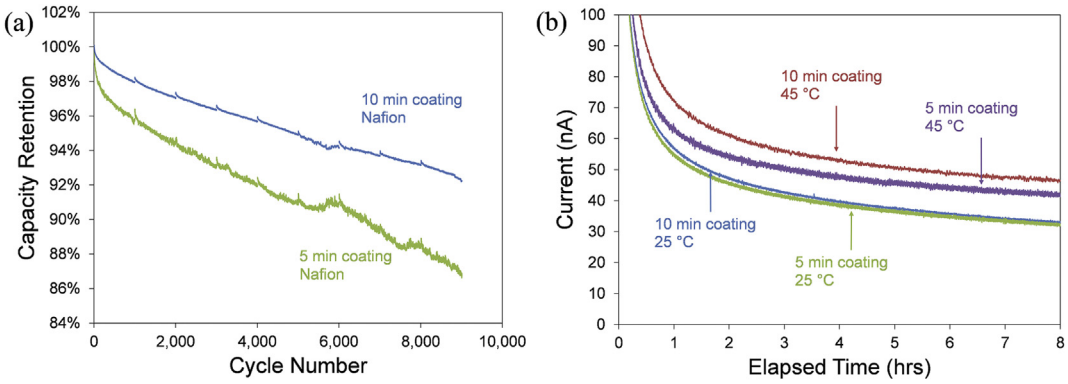

Fig. 6. (a) Cycle lifetime of devices tested in Nafion electrolyte (25 °C and 80% RH) at 25 μA or 3.3 mA cm^{-2}. Cycle lifetime was evaluated following rate capability testing on the same devices. (b) Leakage current at 800 mV for devices tested in Nafion electrolyte at 25 °C and 80% RH as well as 45 °C and 80% RH.

that of the electrodes coated for 10 min was 38%. The TiN plays an import role in the chemical stability of the electrodes, but the resistivity of TiN is much higher than other ductile metals and introduces an undesirable resistance. The improved performance of the devices with longer coating time is believed to be due to increased electronic conductivity of the interdigitated electrode fingers with a thicker RuO_2 layer.

After rate capability testing, the cycle lifetime of supercapacitors in Nafion electrolyte was measured at constant current charge/discharge of 25 μA or 3.3 mA cm^{-2}. Unlike devices tested in aqueous H_2SO_4 electrolyte, the devices did not fail even after 9000 cycles (Fig. 6 (a)). The EIS results in Fig. 7 (a, b) demonstrated a positive relationship between the number of cycles and both the charge transfer and the uncompensated resistance parameters, indicated by the semi-circle diameter and high frequencies and the real impedance value at the highest measured frequency, respectively. The uncompensated resistance increase is due to the limited conductivity of the solid electrolyte governed by the diffusion processes in Nafion. The increasing values of the charge transfer resistance are due to a gradual and mild material failing process that was supported also by the gradual decrease in the capacity retention. After increasing the temperature from 25 °C to 45 °C, the EIS results in Fig. 7 (c, d) show an increase in the uncompensated resistance, but not necessarily the polarization resistance. This seems to imply that the conductivity of solid electrolyte is adversely affected, while the interface between electrode and

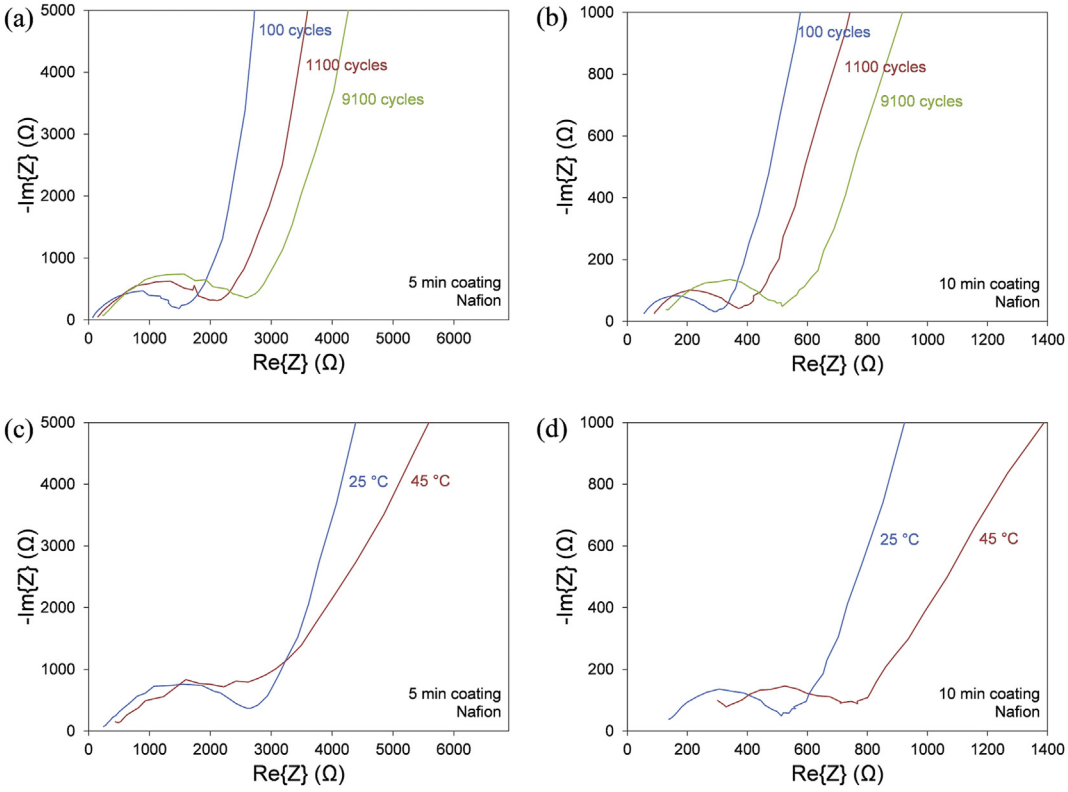

Fig. 7. Impedance spectroscopy evolution during cycle lifetime testing for devices in Nafion electrolyte (25 °C and 80% RH) for (a) 5 min coating and (b) 10 min coating. Afterwards, the environmental temperature was increased to 45 °C at 80% RH and the effect of temperature is shown for (c) 5 min coating and (d) 10 min coating. The electrodes were tested at 10 mV AC amplitude from 100 kHz to 10 mHz.

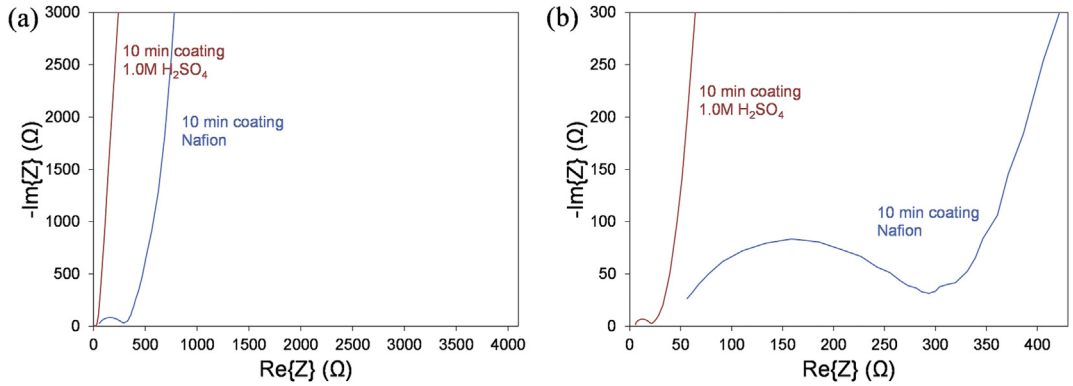

Fig. 8. (a) Impedance spectroscopy comparison between aqueous 1.0M H_2SO_4 and solid Nafion electrolyte (25 °C and 80% RH). The electrodes were tested at 10 mV AC amplitude from 100 kHz to 10 mHz. A close-up of the lower left of the graph is provided in (b).

electrolyte is not. Nevertheless, the properties of solid Nafion electrolyte at various relative humidities and temperatures have been carefully studied [30], and the conductivity of Nafion was reported to increase slightly for conditions comparable to this work. One is left to conclude that a structural change is occurring in the TMV-1Cys/RuO_2 coated titanium nitride microelectrodes, and a partial failure at the interface between the TiN and RuO_2 layers, resulting in increased equivalent series resistance, is a possibility.

The performance limit of the TMV-1Cys templated RuO_2 micro-supercapacitors may be diffusion in the electrolyte, diffusion within the $RuO_2 \cdot xH_2O$ active material or electronic conduction in the current collector. The diffusivity of H^+ ions in water is approximately 2×10^{-5} cm^2 sec^{-1} at room temperature [32], however the diffusivity in Nafion is slower: approximately 5×10^{-6} cm^2 sec^{-1} at 80% relative humidity [30]. Since the diffusivity is highly dependent on relative humidity, the devices were tested in a controlled environment at 80% RH. Measurement of the proton diffusivity in RuO_2 has been reported to be 6×10^{-14} cm^2 sec^{-1} for powder treated at 200 °C [33] and 5×10^{-15} cm^2 sec^{-1} for powder treated at 450 °C [34]. The transport mechanism in $RuO_2 \cdot xH_2O$ has been discussed by Dmowski et al. [4] and involves the diffusion of ions along nanocrystalline boundaries, which is much faster than bulk diffusion. A detailed study of $RuO_2 \cdot xH_2O$ by impedance spectroscopy [35] reported diffusion values between 1×10^{-11} and 1×10^{-12} cm^2 sec^{-1}. When tested in liquid electrolyte a doubling of coating time increased capacity by ca. 40%, but in Nafion the capacity increased by only ca. 25%. The additional mass from longer coatings is likely not available for reduction/oxidation due to the kinetic limitations of the solid electrolyte. This conclusion is supported by a significantly larger charge transfer and uncompensated resistances in Nafion electrolyte than in aqueous 1.0M H_2SO_4 electrolyte due to lower ion diffusion rates, as shown in a comparison of Nyquist plots in Fig. 8. A detailed discussion of Nafion as a supercapacitor electrolyte can be found in Lufrano et al. [36]. A notable difference between this work and other work using Nafion membranes (for use in applications with both faradaic and non-faradaic processes) is the lack of an acid wash step since the deposited Nafion film would swell and delaminate from the micro-supercapacitor electrodes. This wash step is usually performed to improve ionic conductivity by removing metallic cations from the ionomer, therefore the Nafion electrolyte used here may have lower than ideal ionic conduction.

Finally, the leakage current of the described device with solid electrolyte was measured to be as low as 32 nA after 8 h when held at a voltage of 800 mV (see Fig. 6 (b)). This is an excellent value considering that commercially available supercapacitors have leakage currents of approximately 1 μA [37] to 5 μA [38], and the values for aluminum electrolytic capacitors are significantly higher. It is expected that the micro-supercapacitors can be scaled up in parallel configurations for increased total capacitance while retaining low leakage characteristics.

4. Conclusions

Micro-supercapacitors with a 3D hierarchical electrode with micro- and nano-length scales have been fabricated based on the TMV-1Cys bio-template with a conformal RuO_2 coating. Excellent values for areal capacitance as high as 203 mF cm^{-2} were measured with Nafion solid electrolyte. A self-assembly method of TMV-1Cys has been combined with selective coating of hydrated RuO_2 on metallic electrodes with sacrificial Ni leading to a robust and efficient process integration strategy. The low leakage current and high rate capability of these micro-supercapacitors are conducive to applications in energy-harvesting and pulse-power delivery. The extremely small size (the device shown in Fig. 2 without electrolyte is only 10 um thick) will lead to micro-supercapacitors with high energy and power density. Future work entails the patterning and encapsulation of Nafion solid electrolyte using a layer to prevent absorbed water from escaping in low humidity environments with the goal of a micro-supercapacitor fully integrated into a flexible polyimide device process.

Acknowledgments

This work has been supported by the Laboratory for Physical Sciences (LPS), and the authors would like to acknowledge the excellent clean room support team at LPS. The authors would also like to thank Dr. Konstantinos Gerasopoulos and Dr. Ekaterina Pomerantseva for constructive discussions and for their contributions to this work. This work was supported as part of the Nanostructures for Electrical Energy Storage (NEES), an Energy Frontier Research Center funded by the U.S. Department of Energy, Office of Science, Basic Energy Sciences, under award number DESC0001160.

References

[1] J.P. Zheng, T.R. Jow, A new charge storage mechanism for electrochemical capacitors, J. Electrochem. Soc. 142 (1995) L6–L8, http://dx.doi.org/10.1149/1.2043984.
[2] J.P. Zheng, P.J. Cygan, T.R. Row, Hydrous ruthenium oxide as an electrode material for electrochemical capacitors, J. Electrochem. Soc. 142 (1995) 2699–2703, http://dx.doi.org/10.1149/1.2050077.
[3] D.A. McKeown, et al., Structure of hydrous ruthenium oxides: implications for charge storage, J. Phys. Chem. B 103 (1999) 4825–4832, http://dx.doi.org/10.1021/jp990096n.
[4] W. Dmowski, T. Egami, K.E. Swider-Lyons, C.T. Love, D.R. Rolison, Local atomic

structure and conduction mechanism of nanocrystalline hydrous RuO_2 from X-ray scattering, J. Phys. Chem. B 106 (2002) 12677–12683, http://dx.doi.org/10.1021/jp026228l.
[5] W. Sugimoto, H. Iwata, K. Yokoshima, Y. Murakami, Y. Takasu, Proton and electron conductivity in hydrous ruthenium oxides evaluated by electrochemical impedance spectroscopy: the origin of large capacitance, J. Phys. Chem. B 109 (2005) 7330–7338, http://dx.doi.org/10.1021/jp044252o.
[6] Z. Yuan, R. Puddephatt, Low-temperature chemical vapor deposition of ruthenium dioxide from ruthenium tetroxide: a simple approach to high-purity RuO_2 films, Chem. Mater. 5 (1993) 908–910, http://dx.doi.org/10.1021/cm00031a004.
[7] K.E. Swider-Lyons, C.T. Love, D.R. Rolison, Selective vapor deposition of hydrous RuO_2 thin films, J. Electrochem. Soc. 152 (2005) C158–C162, http://dx.doi.org/10.1149/1.1859713.
[8] J.P. Zheng, Ruthenium oxide-carbon composite electrodes for electrochemical capacitors, Electrochem. Solid-State Lett. 2 (1999) 359–361, http://dx.doi.org/10.1149/1.1390837.
[9] H. Kim, B.N. Popov, Characterization of hydrous ruthenium oxide/carbon nanocomposite supercapacitors prepared by a colloidal method, J. Power Sour. 104 (2002) 52–61, http://dx.doi.org/10.1016/S0378-7753(01)00903-X.
[10] C.-C. Hu, W.-C. Chen, K.-H. Chang, How to achieve maximum utilization of hydrous ruthenium oxide for supercapacitors, J. Electrochem. Soc. 151 (2004) A281–A290, http://dx.doi.org/10.1149/1.1639020.
[11] C.-C. Hu, K.-H. Chang, M.-C. Lin, Y.-T. Wu, Design and tailoring of the nanotubular arrayed architecture of hydrous RuO_2 for next generation supercapacitors, Nano Lett. 6 (2006) 2690–2695, http://dx.doi.org/10.1021/nl061576a.
[12] N. Kang, T. Yu, G.-H. Lim, T. Koh, B. Lim, Facile synthesis of carbon-supported, ultrasmall ruthenium oxide nanocrystals for supercapacitor electrode materials, Chem. Phys. Lett. 592 (2014) 192–195, http://dx.doi.org/10.1016/j.cplett.2013.12.020.
[13] V. Subramanian, S.C. Hall, P.H. Smith, B. Rambabu, Mesoporous anhydrous RuO2 as a supercapacitor electrode material, Solid State Ion. 175 (2004) 511–515, http://dx.doi.org/10.1016/j.ssi.2004.01.070.
[14] W. Sugimoto, K. Yokoshima, Y. Murakami, T. Takasu, Charge storage mechanism of nanostructured anhydrous and hydrous ruthenium-based oxides, Electrochim. Acta 52 (2006) 1742–1748, http://dx.doi.org/10.1016/j.electacta.2006.02.054.
[15] X. Zhao, B. Mendoza Sanchez, P.J. Dobson, P.S. Grant, The role of nanomaterials in redox-based supercapacitors for next generation energy storage devices, Nanoscale 3 (2011) 839–855, http://dx.doi.org/10.1039/c0nr00594k.
[16] C.-C. Liu, et al., Planar ultracapacitors of miniature interdigital electrode loaded with hydrous RuO_2 and RuO_2 nanorods, Electrochim. Acta 55 (2010) 5768–5774, http://dx.doi.org/10.1016/j.electacta.2010.05.015.
[17] D. Pech, et al., Influence of the configuration in planar interdigitated electrochemical micro-capacitors, J. Power Sour. 230 (2013) 230–235, http://dx.doi.org/10.1016/j.jpowsour.2012.12.039.
[18] X. Wang, Y. Yin, X. Li, Z. You, Fabrication of a symmetric micro supercapacitor based on tubular ruthenium oxide on silicon 3D microstructures, J. Power Sour. 252 (2014) 64–72, http://dx.doi.org/10.1016/j.jpowsour.2013.11.109.
[19] X. Wang, Y. Yin, C. Hao, Z. You, A high-performance three-dimensional micro supercapacitor based on ripple-like ruthenium oxide–carbon nanotube composite films, Carbon 82 (2015) 436–445, http://dx.doi.org/10.1016/j.carbon.2014.10.087.
[20] A.B. LaConti, S. Sarangapani, J.A. Kosek, J. Forchione, Proton exchange membrane electrochemical capacitors and fuel cells for pulse power applications, in: Power Sources Symposium, 1992., IEEE 35th International, Cherry Hill, NJ, 1992, pp. 298–301, http://dx.doi.org/10.1109/IPSS.1992.281997.
[21] K.-W. Park, H.-J. Ahn, Y.-E. Sung, All-solid-state supercapacitor using a Nafion polymer membrane and its hybridization with a direct methanol fuel cell, J. Power Sour. 109 (2002) 500–506, http://dx.doi.org/10.1016/S0378-7753(02)00165-9.
[22] W. Sun, X. Chen, Fabrication and tests of a novel three dimensional micro supercapacitor, Microelectron. Eng. 86 (2009) 1307–1310, http://dx.doi.org/10.1016/j.mee.2008.12.010.
[23] C. Shen, X. Wang, W. Zhang, F. Kang, A high-performance three-dimensional micro supercapacitor based on self-supporting composite materials, J. Power Sour. 196 (2011) 10465–10471, http://dx.doi.org/10.1016/j.jpowsour.2011.08.007.
[24] H. Durou, et al., Wafer-level fabrication process for fully encapsulated micro-supercapacitors with high specific energy, Microsyst. Technol. 18 (2012) 467–473, http://dx.doi.org/10.1007/s00542-011-1415-7.
[25] E. Royston, A. Ghosh, P. Kofinas, M.T. Harris, J.N. Culver, Self-assembly of virus-structured high surface area nanomaterials and their application as battery electrodes, Langmuir 24 (2008) 906–912, http://dx.doi.org/10.1021/la7016424.
[26] K. Gerasopoulos, et al., Biofabrication methods for the patterned assembly and synthesis of viral nanotemplates, Nanotechnology 21 (2010) 055304, http://dx.doi.org/10.1088/0957-4484/21/5/055304.
[27] M. Gnerlich, et al., Solid flexible electrochemical supercapacitor using Tobacco mosaic virus nanostructures and ALD ruthenium oxide, J. Micromech. Microeng. (2013) 114014, http://dx.doi.org/10.1088/0960-1317/23/11/114014.
[28] X.Z. Fan, et al., Tobacco mosaic virus: a biological building block for micro/nano systems, J. Vac. Sci. Technol. A 31 (2013) 050815, http://dx.doi.org/10.1116/1.4816584.
[29] R. Thiruvengadathan, et al., Nanomaterial processing using self-assembly-bottom-up chemical and biological approaches, Rep. Prog. Phys. 76 (2013) 066501, http://dx.doi.org/10.1088/0034-4885/76/6/066501 (54pp).
[30] S. Ochi, O. Kamishima, J. Mizusaki, J. Kawamura, Investigation of proton diffusion in Nafion®117 membrane by electrical conductivity and NMR, Solid State Ion. 180 (2009) 580–584, http://dx.doi.org/10.1016/j.ssi.2008.12.035.
[31] M.D. Stoller, R.S. Ruoff, Best practice methods for determining an electrode material's performance for ultracapacitors, Energy Environ. Sci. 3 (2010) 1294–1301, http://dx.doi.org/10.1039/c0ee00074d.
[32] S.H. Lee, J.C. Rasaiah, Proton transfer and the mobilities of the H^+ and OH^- ions from studies of a dissociating model for water, J. Chem. Phys. 135 (2011) 124505, http://dx.doi.org/10.1063/1.3632990.
[33] G.T. Yu, S.K. Yen, A novel method to determine the diffusion coefficient of hydrogen ion in ruthenium oxide films, Chem. Phys. Lett. 364 (2002) 517–521, http://dx.doi.org/10.1016/S0009-2614(02)01399-4.
[34] J.E. Weston, B.C.H. Steele, Proton diffusion in crystalline ruthenium dioxide, J. Appl. Electrochem 10 (1980) 49–53, http://dx.doi.org/10.1007/BF00937337.
[35] J. Rishpon, S. Gottesfeld, Resolution of Fast and Slow Charging Processes in Ruthenium Oxide Films: An AC Impedance and Optical Investigation, J. Electrochem. Soc. 131 (1984) 1960–1968, http://dx.doi.org/10.1149/1.2116000.
[36] F. Lufrano, P. Staiti, Performance improvement of Nafion based solid state electrochemical supercapacitor, Electrochim. Acta 49 (2004) 2683–2689, http://dx.doi.org/10.1016/j.electacta.2004.02.021.
[37] Murata Manufacturing Co., Electrical Double Layer Capacitor DMF Series. [Online]. http://www.murata.com/en-us/products/capacitor/edlc/dmf.
[38] AVX Corporation, AVX BestCap® Ultra-low ESR High Power Pulse Supercapacitors. [Online]. http://www.avx.com/docs/masterpubs/bestcap.pdf.